RSC Advances

ROYAL SOCIETY OF CHEMISTRY

www.rsc.org/advances

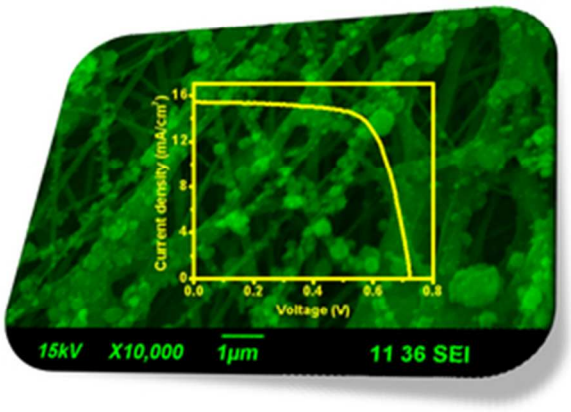

31x23mm (300 x 300 DPI)

An innovative one-dimensional nanoarchitecture having TiO_2 nanoparticles decorating TiO_2 nanofiber surface fabricated by simultaneous electrospinning-electrospraying technique as a photoanode for dye-sensitized solar cells

Journal Name

RSCPublishing

COMMUNICATION

TiO_2 nanoparticles @ TiO_2 nanofibers - an innovative one-dimensional material for dye-sensitized solar cells

Cite this: DOI: 10.1039/x0xx00000x

G. S. Anjusree, T. G. Deepak, K. R. Narendra Pai, John Joseph, T. A. Arun, Shantikumar V Nair and A. Sreekumaran Nair*

Received ooth January 2013,
Accepted ooth .....

DOI: 10.1039/x0xx00000x

www.rsc.org/

We report a unique one-dimensional (1-D) morphology of TiO_2 having TiO_2 nanoparticles decorating the surface of TiO_2 nanofibers fabricated by simultaneous electrospinning and electrospraying technique. The composite made by both nanofibers and nanoparticles is used as a photoanode material for dye-sensitized solar cells (DSCs) which helped in overcoming the limitations associated with nanofibers and nanoparticles when employed separately. The DSC showed an excellent efficiency of 7.89% (for a square-shaped cell of area 0.2 cm^2) in comparison to 6.87 % for the nanoparticulate DSC and 5.21% for the nanofiber DSC (for cells of same area and thickness) which is an impressive value when literature on DSC fabrication with 1-D nanostructures for DSCs is concerned.

The field of 3rd generation solar cells has seen an emerging breakthrough since Grätzel reported the success of dye-sensitized solar cells (DSCs) in 1991.[1-4] DSCs are a multicomponent system which include: a) a photoanode consisting of a metal oxide semiconductor coated on a transparent conducting oxide (TCO, commonly a fluorine-doped tin oxide, FTO), b) a counter electrode consisting of Pt/carbon coated on FTO c) a ruthenium based dye d) an I^-/I_3^- redox electrolyte.[1-4] The commonly used photoanode is a porous TiO_2 layer of 10-15 μm thick which acts as a support for the sensitizers and brings about the electron transport.[1-4] Traditionally two types of TiO_2 nanomaterials are employed in DSCs, mesoporous spherical particles and one-dimensional (1-D) nanostructures such as nanofibers/nanowires/nanorods.[5-7] Both the types of materials have merits and demerits. DSCs are usually fabricated from spherical mesoporous TiO_2 nanostructures having a bilayer configuration (i.e. a mesoporous TiO_2 active layer made up of small particles and a small scattering layer having bigger particles). State-of-the-art DSCs fabricated by this methodology show ~ 10-12% efficiency.[8,9] However, this efficiency is not accessible to researchers across the globe routinely. Also, adding a scattering layer is expensive and technologically complicated when comes to the scale-up of DSCs.[10-12] Further, the photoanodes made of spherical particles of TiO_2 suffer from structural disorders (dead-ends are common in the photoanode array) and trap sites, which reduce the efficiency because of scattering of free electrons with reduced carrier mobility.[5,13] One-dimensional (1-D) TiO_2 nanomaterials have attracted the focus in the recent past because of enhanced electron transport (semi-guided/guided) and reduced number of trapping sites thus offering a smooth transport and collection for the photoinjected electrons.[5-7] Further, the 1-D nanostructures facilitate enhanced light scattering mostly at the red part of the spectrum.[5-7] Despite these appealing aspects, the 1-D TiO_2 nanostructures often suffer from reduced internal surface area and hence insufficient dye adsorption which leads to lower performing cells.[5-7,14,15] In such a scenario, we thought of a unique proposition of having both these nanostructures together in a single nanoarchitecture so that the benefits of both could be harvested.

Electrospraying, sol-gel, hydrothermal[16] etc. are the widely used

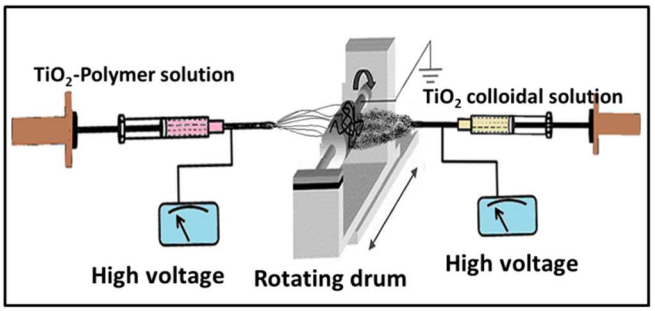

Fig. 1. A schematic of the co-electrospinning-electrospraying set-up used for making fiber-particle composites.

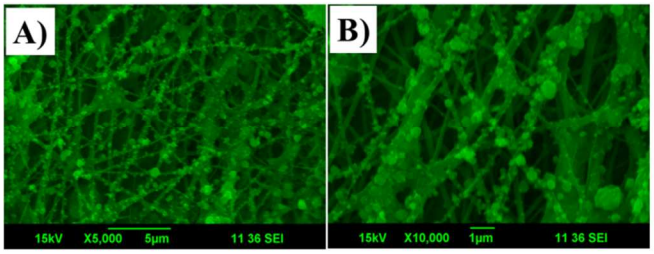

Fig. 2. SEM images of the fiber-particle composites. A & B – low and high magnification images.

methods for the synthesis of nanoparticles. The most versatile method for the preparation of TiO_2 nanofibers is by electrospinning[17,18] although hydrothermal, template-assisted growth, etc. have also been explored in detail. We have selected electrospraying and electrospinning techniques and combined them together in a single experiment to create a unique nanoarchitecture wherein the TiO_2 nanofibers produced by electrospinning have TiO_2 nanoparticles deposited by electrospraying decorating the surface. **To the best of our knowledge, this is the first attempt on use of such nanoarchitecture for DSCs**. However, it must also be mentioned that there exist two reports in literature on DSCs using TiO_2 fiber-particle composites[19,20] which are physical blends of particles and fibers.

Fig. 1 depicts a schematic of the experimental set-up used for simultaneous electrospinning and electrospraying. The as-electrospun fibers (TiO_2 nanoparticle-nanofiber-polymer composite fibers)[21,22] upon sintering (450 ^{0}C for 3h) results in '**TiO_2 nanoparticles @ TiO_2 nanofibers**' architecture (see **ESI 1** also). **Fig. 2** shows a low-magnified (A) and resolved (B) SEM image of the TiO_2 fiber-particle architecture. The TiO_2 particles on the surfaces of the fibers were aggregated and have sizes ranging from 50-500 nm while the fibers had diameters ranging from 100-300 nm. The fiber-particle composites were also characterized by TEM (**Fig. 3A&B**). **Fig. 3A** shows the TEM image of the aggregated TiO_2 nanoparticles on the fiber

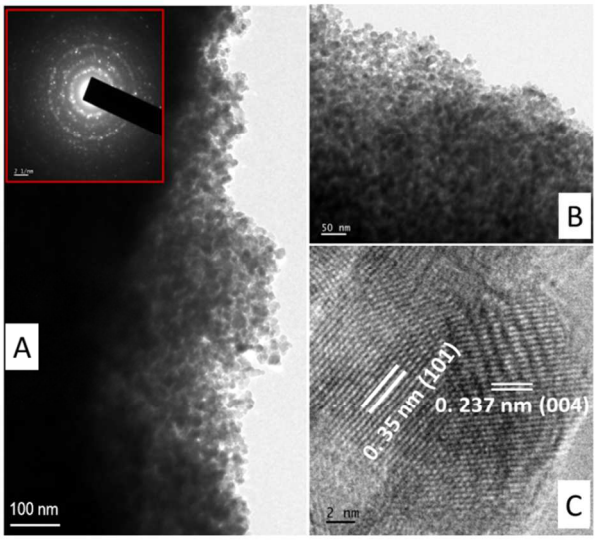

Fig. 3. A- TEM image of the single fiber showing the presence of large number of particles decorating the surface. B- an enlarged view of the nanoparticles on the fiber surface. C- a lattice resolved image of the particles. Inset of A- an SAED pattern revealing the polycrystalline nature of the composite.

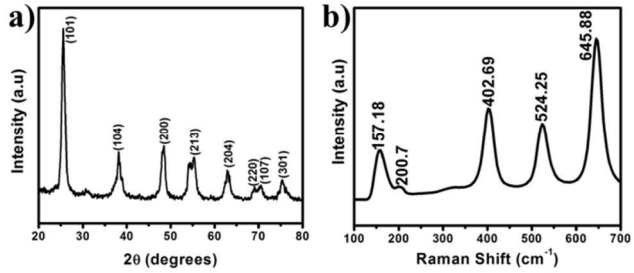

Fig. 4. Powder XRD (a) and Raman (b) spectra of the TiO_2 composite. Peaks are indexed in the spectra itself.

backbone. It is obvious from the images that the aggregated nanoparticles are made up of small spherical nanoparticles of 10-20 nm sizes (**Fig. 3B**). **Fig. 3C** shows a lattice-resolved TEM image showing the (101) lattice orientation of the TiO_2 with the interplanar distance corresponding to 0.35 nm which is in agreement with the pure anatase phase TiO_2. The high crystallinity of the TiO_2 was evident from the selected area electron diffraction (SAED) pattern given (inset of **Fig. 3A**). The TiO_2 was further characterized by powder XRD, Raman and XPS measurements. The XRD pattern (**Fig. 4a**) confirms the pure anatase nature of the TiO_2 (JCPDS No. 21-1272) and its polycrystalline nature. The Raman spectrum of the TiO_2 is shown in **Fig. 4b**. The Raman spectrum of the anatase single crystals, as reported by Ohsaka et al. and Swamy et al.,[23,24] respectively, shows six Raman active modes (A1g+2B1g+3Eg) appearing at 144 cm^{-1} (Eg), 197 cm^{-1} (Eg), 399 cm^{-1} (B1g), 513 cm^{-1} (A1g), 519 cm^{-1} (B1g) and 639 cm^{-1} (Eg), respectively. The respective Raman peaks in the present case appear at 157 cm^{-1}, 200 cm^{-1}, 402 cm^{-1}, 524 cm^{-1} and 645 cm^{-1}, respectively, which are red-shifted in comparison to those of the single crystals. The shift of the Raman peaks to higher wavenumbers could be because of the phonon confinement within the nanoparticles (the size effects) and the associated increase in the photon distribution/dispersion.[23,24] The peak at 524 cm^{-1} could be the combination of (A1g+B1g) which is indicative of the Ti-O stretching type vibration.[23,24] The XPS analysis was also used to confirm the chemical composition and oxidation

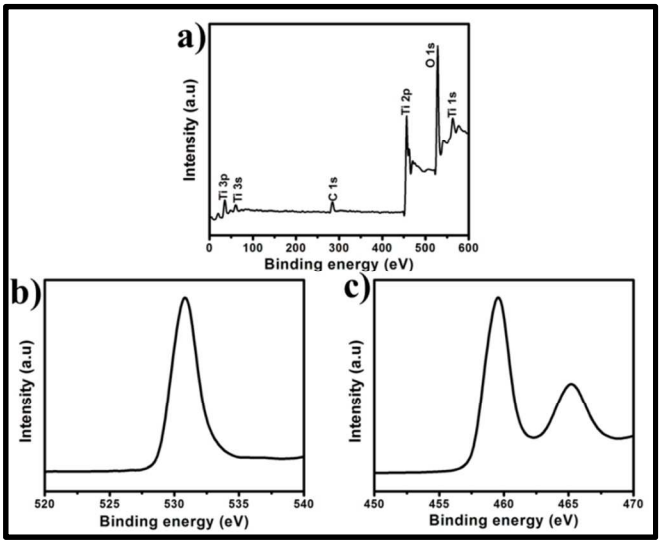

Fig. 5. XPS survey spectrum of the TiO_2 composite (a) and the high-resolution spectra of the elements (b&c).

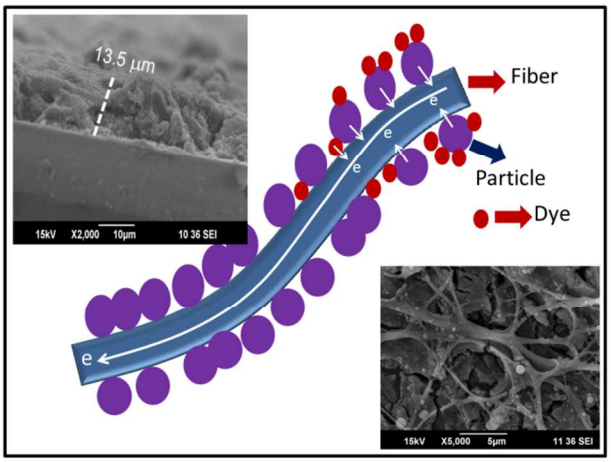

Fig. 6. A cartoon showing the guided electron transport through the fiber-particle composite. The figure is not drawn to scale. Insets- top: cross-sectional SEM image, bottom: an enlarged view from the electrode surface.

state of the elements in the fiber-particle composite. The survey spectrum showing the elemental composition (Ti and O) and high-resolution spectra of the elements are given in **Fig. 5**. The Ti in the TiO_2 showed the Ti 2p (3/2) and Ti 2p (1/2) binding energy peaks at 459.56 eV and 464.19 eV, respectively, corresponding to a spin-orbit coupling of 5.63 eV. The binding energy of O1s was at 530.8 eV and is a single peak corresponding to that of O_2^{-}.[25] The XPS further implies the absence of impurities in the TiO_2.

As we have briefly mentioned in the introduction, the nanoarchitecture fabricated in the present case combines the benefits of both the spherical particles and the 1-D nanofibers. The architecture can facilitate smooth transport and collection of the photoexcited electrons from dyes (bound to both the particle- and fiber surfaces, **Fig. 6,** insets of **Fig. 6** show the cross-sectional SEM image of the electrode and an enlarged view of its surface). We thus felt that the material could be a potential candidate for DSC applications. The DSCs with different thicknesses for the active layer were fabricated and tested as explained in the experimental section. The respective photovoltaic parameters were summarized in **Table 1**. It is evident from **Table 1** that 14 μm is the optimum thickness needed for best DSC performance with the current material. The DSC performance of the composite was compared against that of electrospun TiO_2 nanofibers and the nanoparticles (**Fig. 7 (A&B)**). The DSC made using the composite with a layer thickness of 14 μm achieved a short-circuit current density (Jsc) of 12.98 mA/cm^2 and an energy conversion efficiency (η) of ~7.9%. In comparison, the DSC fabricated using TiO_2 nanoparticles alone (14 μm thick, see **ESI 1** for the TEM image of the particles) had Jsc and η values of 12.67 mA/cm^2 and 6.87%, respectively, whereas the same fabricated with the nanofibers alone (14 μm thick, see **ESI 2** for the TEM image of the TiO_2 nanofibers) shown a Jsc and η of 8.70 mA/cm^2 and 5.21%, respectively. The V_{oc} was found to be varying in the order: fiber-particle composite (0.81 V) > fiber (0.78 V) > particle (0.73 V) whereas the fill-factor was nearly the same for the fiber and fiber-particle composite systems (higher than that of the particle- based) which is because of their less internal resistance (because of their one-dimensional architecture). A summary of the photovoltaic parameters of the DSCs made from fibers, particles and fiber-particle composites of same thickness is given in **Table 2**.

Table 1: Table showing the DSC characteristics at different thicknesses.

Thickness (μm)	V_{oc} (V)	J_{sc} (mA/cm^2)	Fill factor, FF (%)	Efficiency (η, %)
11	0.77	12.4	70.8	6.76
14	0.81	12.98	75.48	7.89
18	0.74	12.17	64.63	6.07
20	0.725	11.9	63.3	5.65

Table 2. A summary of the photovoltaic parameters of the DSCs made from fibers, particles and fiber-particle composites (of same thickness).

Morphology	V_{oc} (V)	J_{sc} (mA/cm^2)	Fill Factor (%)	Efficiency (%)
Fiber	0.78	8.70	75.33	5.21
Particle	0.73	12.67	73.75	6.87
Fiber-particle	0.81	12.98	75.48	7.89

Fig. 7B shows the incident photon-to-electron conversion efficiency (IPCE) spectra from which it is clear that out of the three DSCs; the one made with the fiber-particle composite gave a maximum IPCE of 74% (at 530 nm) compared to the other two (60% for the particle-based and 40% for the fiber-based one). The most important factors contributing to the IPCE are light harvesting efficiency, and charge separation and collection yields. We have analyzed which of these factors was responsible for the *I-V*/IPCE enhancement for the present material. Dye-deloading experiments revealed that the amount of dyes loaded in the DSCs were of the order: particles (1.73×10^{-7} mol/cm^2) > fiber-particle composite (1.69×10^{-7} mol/cm^2 > fibers (6.98×10^{-8} mol/cm^2). Thus it is obvious that high dye loading was not the reason for the enhanced IPCE of the fiber-particle DSC. The overall one-dimensionality of the fiber-particle composite (coupled with the reasonably good dye loading) must have facilitated a smooth charge transport and collection of the photoexcited electrons in the TiO_2 and hence lesser recombinations with the I_3^- species. The effect of enhanced scattering by the composite (especially in the red part of the solar spectrum) must have contributed to the light harvesting efficiency as well by extending the distance that the light travels within the photoelectrode film and hence making more solar photons to get absorbed by the dye molecules.[26]

This was additionally confirmed by a relative estimation of the parallel resistance of the DSCs from the slope of the *I-V* graph near the Voc (**Fig. 7A**). The decrease in the slope implies increase in the parallel resistance of the cell which further implies retardation of the back electron transfer to the I_3^- ions in the electrolyte.[27,28] Thus, the *I-V* trace of the DSC with the fiber-particle system showed a decreased dark current implying relatively less back electron transfer to the I_3^- ions in comparison to the electrodes from the other two materials (the fibers and particles separately).

It must be noted that the TiO_2 photoelectrode fabricated by co-electrospinning-electrospraying is unique and has not been reported to be used for DSCs in literature. There are two reports on nanofiber/nanowire-particle composites,[19,20] both of which employed physical blends of the two components and do not have the overall one-dimensional morphology as reported in the present case. Joshi et al.[20] reported an efficiency of 8.8% from a 7.7 μm thick TiO_2 film comprising 15 wt.% of the nanofibers

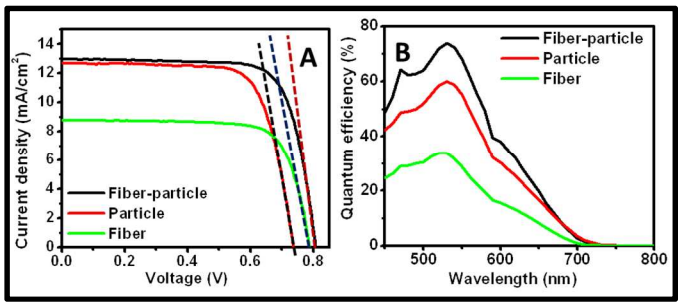

Fig. 7. A- a comparison of the I-V characteristics of the DSCs made out of the fiber-particle composite, fiber and particles. B- the respective IPCE characteristics.

(*i.e.* remaining 85% nanoparticles). This is a nanoparticle-majority system in which nanowires in minority are scattered randomly. Being a physical blend of both, Joshi et al. could optimize the relative amounts of both the components in the composite to have the best efficiency. However, the efficiency in the present case is only ~ 7.9%, a probable reason for which could be that the present system is rich in fibers and particles are only in minority decorating the fiber surface. However, we anticipate that an improvement in efficiency from the current value is possible by further increasing the loading of TiO_2 particles on the fibers. Since the two material systems under consideration are different, a direct comparison of their efficiencies may not be appropriate as well. It must be noted that the present efficiency of ~ 7.9% is one of the impressive values in the category of oriented TiO_2 nanotubes/wires or electrospun TiO_2 in DSCs.[29-32]

Further investigations are needed using electrochemical impedance spectroscopy, open-circuit voltage decay and lifetime measurements to understand the charge transport mechanism and the electron lifetime in the TiO_2 network, etc. The nanoparticle loading on fibers also needs to be optimized for realizing the highest efficiency obtainable from the system. We believe; these will constitute contents for a full paper.

Conclusions

In conclusion, we have fabricated a unique nanoarchitecture having TiO_2 particles decorating the surface of TiO_2 nanofibers by 'co-electrospinning and electrospraying' followed by a high temperature sintering. The composite TiO_2 was characterized by spectroscopy and microscopy. A square-shaped 14 μm thick DSC of area 0.2 cm^2 fabricated out of the material showed an efficiency of 7.9% and IPCE maximum of 74% at ~ 530 nm. Further studies such as electrochemical impedance spectroscopy and electron lifetime measurements are needed to establish the charge transport mechanism through the nanostructures which are currently underway. We believe that with further optimization of the current material such as by increasing the loading of particles on the fibers; the DSC efficiency could be scaled-up to ~ 10%. The experimental technique employed (electrospinning-electrospraying) is scalable using multi-needle electrospinning/spraying setups and hence facile fabrication of the TiO_2 composite is feasible.

Acknowledgement

The Ministry of New and Renewable Energy (MNRE) and Department of Science and Technology (DST), Govt. of India are acknowledged for financial support.

Notes and references

Nanosolar Division, Amrita Centre for Nanosciences & Molecular Medicine, Amrita Institute of Medical Sciences, AIMS Ponekkara PO, Kochi 682041, Kerala, India.
Corresponding author email: sreekumarannair@aims.amrita.edu

1 B. O'regan, and M. Grätzel, *Nature*, 1991, **353**, 737-740.
2. M. Grätzel, *J. Photochem. Photobiol., C* 2003, **4**, 145-153.
3. L. M. Gonçalves, V. de Zea Bermudez, H. A. Ribeiro, and A. M. Mendes, *Energy Environ. Sci.*, 2008, **1**, 655-667.
4. A. Hagfeldt, G. Boschloo, L. Sun, L. Kloo, and H. Pettersson, *Chem. Rev.*, 2010, **110**, 6595-6663.
5. K. Zhu, N. R. Neale, A. Miedaner, and A. J. Frank, *Nano Lett.*, 2007, **7**, 69-74.
6. A. S. Nair, Z. Peining, V. J. Babu, Y. Shengyuan, and S. Ramakrishna, *Phys. Chem. Chem. Phys.*, 2011, **13**, 21248- 21261.
7. N. G Park, J. Lagemaat, A. J. Frank, *J. Phys. Chem. B,* 2000, **104**, 8989-8994.
8. S. Ito, T. N. Murakami, P. Comte, P. Liska, M. Grätzel, M. K. Nazeeruddin, M. Grätzel, *Thin Solid Films*, 2008, **516**, 4613-4619.
9. Y. Chiba, A. Islam, Y. Watanabe, R. Komiya, N. Koide, and L. Han, *Jpn. J. Appl. Phys.*, 2006, **45**, L638-L640.
10. F. Sauvage, D. Chen, P. Comte, F. Huang, L.-P. Heiniger, Y.-B. Cheng, R. A. Caruso, and M. Grätzel, *ACS Nano*, 2010, **4**, 4420-4425.
11. D. Chen, F. Huang, Y.-B. Cheng, and R. A. Caruso, *Adv. Mater.*, 2009, **21**, 2206-2210.
12. Z. Peining, W. Yongzhi, M. V. Reddy, A. S. Nair, P. Shengjie, N. Sharma, V. K. Peterson, B. V. R. Chowdari, and S. Ramakrishna, *RSC Adv.*, 2012, **2**, 5123-5126.
13. J. R. Jennings, A. Ghicov, L. M. Peter, P. Schmuki, and A. B. Walker, *J. Am. Chem. Soc.*, 2008, **130**, 13364- 13372.
14. D. Kuang, J. Brillet, P. Chen, M. Takata, S. Uchida, H. Miura, K. Sumioka, S. M. Zakeeruddin, and M. Grätzel, *ACS Nano*, 2008, **2**, 1113-1116.
15. P. Roy, D. Kim, K. Lee, E. Spiecker, and P. Schmuki, *Nanoscale*, 2010, **2**, 45-59.
16. X. Chen, and S. S. Mao, *Chem. Rev.*, 2007, **107**, 2891-2959.
17. W. E. Teo, and S. Ramakrishna, *Nanotechnology*, 2006, **17**, R89-R106.
18. D. Li, and Y. Xia, *Adv. Mater.*, 2004, **16**, 1151-1170.
19. B. Tan, and Y. Wu, *J. Phys. Chem. B*, 2006, **110**, 15932- 15938.
20. P. Joshi, L. Zhang, D. Davoux, Z. Zhu, D. Galipeau, H. Fong, and Q. Qiao, *Energy Environ Sci.*, 2010, **3**, 1507- 1510.
21. G. R. A. Kumara, S. Kawasaki, P. V. V. Jayaweera, E. V. A. Premalal, and S. Kaneko, *Thin Solid Films*, 2012, **520**, 4119-4121.
22. A. S. Nair, R. Jose, Y. Shengyuan, and S. Ramakrishna, *J. Colloid Interface Sci.*, 2011, **353**, 39-45.
23. T. Ohsaka, F. Izumi, and Y. Fujiki, *J. Raman Spectrosc.*, 1978, **7**, 321-324.
24. V. Swamy, A. Kuznetsov, L. S. Dubrovinsky, R. A. Caruso, D. G. Shchukin, and B. C. Muddle, *Phys. Rev. B*, 2005, **71**, 184302-184313.
25. J. Pan, G. Liu, G. Q. Lu, and H. M. Cheng, *Angew. Chem. Int. Ed.*, 2011, **50**, 2133 -2137.

26. Q. Zhang, T. P. Chou, B. Russo, S. A. Jenekhe, and G. Cao, *Angew. Chem. Int. Ed.*, 2008, **47**, 2402-2406.
27. F. Fabregat-Santiago, J. Bisquert, E. Palomares, L. Otero, D. Kuang, S. M. Zakeeruddin, and M. Grätzel, *J. Phys. Chem. C*, 2007, **111**, 6550-6560.
28. Q. Wang, J.-E. Moser, and M. Grätzel, *J. Phys. Chem. B*, 2005, **109**, 14945-14953.
29. Z. Peining, A. S. Nair, Y. Shengyuan, P. Shengjie, N. Elumalai, and S. Ramakrishna, *J. Photochem. Photobiol.*, A 2012, **231**, 9-18.
30. T. Krishnamoorthy, V. Thavasi, G. M. Subodh, and S. Ramakrishna, *Energy Environ. Sci.*, 2011, **4**, 2807-2812.
31. B. H. Lee, M. Y. Song, S.-Y. Jang, S. M. Jo, S.-Y. Kwak, and D. Y. Kim, *J. Phys. Chem. C*, 2009, **113**, 21453-21457.
32. A. S. Nair, P. Zhu, V. J. Babu, Y. Shengyuan, T. Krishnamoorthy, R. Murugan, S. Peng, and S. Ramakrishna, *Langmuir*, 2012, **28**, 6202-6206.